

**Development of a Piezoelectric Actuated Mechanism  
for Flapping Wing Mirco-Aerial-Vehicle Applications**

K. Lal Kummari<sup>1</sup>, D. Li<sup>2</sup>, S. Guo<sup>2</sup>, and Z. Huang<sup>1\*</sup>

<sup>1</sup>Department of Materials, Cranfield University, Beds, MK43 0AL, UK

<sup>2</sup>Department of Aerospace Engineering, Cranfield University, Beds, MK43 0AL, UK

\*Corresponding author e-mail: Z.Huang@Cranfield.ac.uk

**Abstract**

A piezoelectric actuated 2-bar 2-flexure motion amplification mechanism for flapping wing micro aerial vehicle application has been investigated.  $f_r \cdot A$  as an optimization criterion has been introduced where  $f_r$  is its fundamental resonant frequency of the system and  $A$  the vibration amplitude at the wing tip, or the free tip deflection at quasi-static operation. This criterion can be used to obtain the best piezoelectric actuation mechanism with the best energy transmission coefficient for flapping wing MAV applications, and is a measurable quantity therefore can be compared with experimental results. A simplified beam model has been developed to calculate the fundamental resonant frequency for the full system consisted of piezoelectric actuator, motion amplification mechanism and the attached wing and the calculated values were compared with the measured results. A clear trend of the criteria  $f_r \cdot A$  varying with the 2-flexure dimension, stiffness and setting angle has been obtained from the measured data and also the predicted results as a guideline for optimal design of the system.

## 1 Introduction

The interest in flapping wing micro aerial vehicles (MAV) has resulted in substantial work in recent years<sup>1</sup>. As demonstrated by flying birds and insects, flapping flight is advantageous for its superior manoeuvrability and lifting capability at low flight speeds<sup>2</sup>. Piezoelectric materials especially lead zirconate titanate (PZT) are widely used in smart structures as sensors and actuators due to their high bandwidth, high output force, compact size, and high power density<sup>3</sup>. However, the piezoelectric displacement is intrinsically very small therefore some kind of motion amplification mechanisms is required to achieve large deflection. Fearing et al. developed piezoelectrically actuated four-bar mechanisms for micromechanical flying insect thorax<sup>4-6</sup>. Cox et al. reported three piezoelectrically activated four bar and five bar linkage systems for the electromechanical emulation of mesoscale flapping flight<sup>7</sup>. Park et al. developed a four bar linkage system driven by lightweight piezo-composite actuator to mimicking the flapping wing system of insects<sup>8</sup>.

The optimization of piezoelectric actuated mechanisms is not straight forward since the optimization criterion is application dependent and can vary among optimal mode shape and frequency, tip deflection, and maximal electromechanical coupling factor (EMCF)... etc. Wang et al. investigated the electromechanical coupling and output efficiency of piezoelectric bimorph and unimorph actuators in terms of maximization of three actuator characteristic parameters, namely electromechanical coupling coefficient, energy transmission coefficient and mechanical output energy for quasi-static operation<sup>9,10</sup>.

The Strouhal Number is used in the analysis of the flapping wing efficiency in a oscillating, unsteady flow dynamics<sup>11</sup>. It can be expressed as  $St = f \cdot A / U$ , which divides stroke frequency ( $f$ ) and amplitude ( $A$ ) by forward speed ( $U$ ).  $St$  is known to govern a well-defined series of vortex growth and shedding regimes and propulsive efficiency is high over a narrow range of  $St$  and usually peaks within the interval  $0.2 < St < 0.4$ . Most swimming and flying animals when cruising operate at  $0.2 < St < 0.4$ <sup>12</sup>. This can be used for the prediction of cruising flight and swimming speed for animals as  $U = f \cdot A / St$ , and can also be used as design guide  $f \cdot A = U \cdot St$  for wing morphology and kinematics in MAV application, where  $St \approx 0.3$ <sup>12</sup>. It has been demonstrated that  $f_r \cdot A$  can be used as an optimization criterion for piezoelectric fans where  $f_r$  is its fundamental resonant frequency and  $A$  the vibration amplitude at the resonant frequency, or the free tip deflection at quasi-static operation<sup>13</sup>. In this report we use  $f \cdot A$  as the optimization criterion for compliance motion amplification mechanisms for flapping wing actuators. Numerical modeling will be used to analyse the performance of the system, and these theoretical values are compared with measured results.

## **2 Experimental**

A 2-bar 2-flxure mechanism as shown in Figure 1 was investigated in this work. This mechanism was made from strips of pre-prep carbon fibre links glued together by nylon flexures. One bar  $L_2$  is clamped and the other bar  $L_1$  is connected to the piezoelectric actuator. Custom sized actuators cut from THUNDER TH-7R (Face International Inc., USA) were used to drive the mechanism. Wing frame made of carbon fibre reinforced plastic strips was covered with polymer thin foils as wing skin

and the whole wing was attached to the mechanism, the dimensions of the wing frame was 70 mm x 20 mm. The width for the carbon fibres and the nylon was 5 mm.

For numerical beam modelling to calculate the resonant frequency, the weight and length of each component section was measured. Mass was considered distributed uniformly at each section along the wing span. The exact geometry of the wing was not considered since the aerodynamic resistance on the wing will reduce the vibration amplitude only and have little effect on its resonant frequency<sup>14</sup>.

A peak-to-peak voltage of 340V AC (-170 to +170V) was applied to the cut THUNDER TH-7R actuator. A high speed camera (Photron APX) with frame rate of 2000 frames/s was used to record the dynamic motion of the wing tip. The camera was controlled by a computer system to record images of the vibration continuously for about one second, collecting just over 2000 images, which covered several full cycles of the vibration. The displacement data were obtained by comparing images over a full cycle and directly measuring the images showing the largest displacement<sup>13</sup>.

### **3 Results and Discussion**

#### **3.1 Characterisation and numerical modelling of the cut THUNDER actuator**

The THUNDER TH-7R actuators were chosen for their high performance and robustness. Initial tests indicated that TH-7R was too large in size and had a too high resonant frequency, hence each TH-7R was cut into four equal sized smaller strips. So the width of the actuator was 19 mm, and the dome height was measured as 7.3 mm, (the data supplied by the manufacturer was 9.55 mm though). In order to be able to

model the resonant frequency of the whole system, the performance of the cut TH-7R need to be modelled first. Basic properties of the materials used are summered in Table 1.

The Thunder actuator made of 5 layers of materials bonded together can be modelled as a composite laminated beam. The relations between strain and stress, vector of electric field  $E_i$  and temperature difference  $\Delta T$  of the piezo-actuator device can be expressed as<sup>15,16</sup>

$$\begin{Bmatrix} \varepsilon_1 \\ \varepsilon_2 \\ \varepsilon_3 \\ \gamma_{23} \\ \gamma_{31} \\ \gamma_{12} \end{Bmatrix} = \begin{bmatrix} S_{11} & S_{12} & S_{13} & 0 & 0 & 0 \\ S_{12} & S_{22} & S_{23} & 0 & 0 & 0 \\ S_{13} & S_{23} & S_{33} & 0 & 0 & 0 \\ 0 & 0 & 0 & S_{44} & 0 & 0 \\ 0 & 0 & 0 & 0 & S_{55} & 0 \\ 0 & 0 & 0 & 0 & 0 & S_{66} \end{bmatrix} \begin{Bmatrix} \sigma_1 \\ \sigma_2 \\ \sigma_3 \\ \tau_{23} \\ \tau_{31} \\ \tau_{12} \end{Bmatrix} + \begin{bmatrix} 0 & 0 & d_{31} \\ 0 & 0 & d_{32} \\ 0 & 0 & d_{33} \\ 0 & d_{24} & 0 \\ d_{15} & 0 & 0 \\ 0 & 0 & 0 \end{bmatrix} \begin{Bmatrix} E_1 \\ E_2 \\ E_3 \end{Bmatrix} + \begin{Bmatrix} \alpha_1 \\ \alpha_2 \\ \alpha_3 \\ 0 \\ 0 \\ 0 \end{Bmatrix} \Delta T \quad (1)$$

In the 1-2 plane, the above strain-stress equation under plane stress can be reduced as

$$\begin{Bmatrix} \varepsilon_1 \\ \varepsilon_2 \\ \gamma_{12} \end{Bmatrix} = \begin{bmatrix} S_{11} & S_{12} & 0 \\ S_{12} & S_{22} & 0 \\ 0 & 0 & S_{66} \end{bmatrix} \begin{Bmatrix} \sigma_1 \\ \sigma_2 \\ \tau_{12} \end{Bmatrix} + \begin{bmatrix} d_{31} \\ d_{32} \\ 0 \end{bmatrix} E_3 + \begin{Bmatrix} \alpha_1 \\ \alpha_2 \\ 0 \end{Bmatrix} \Delta T \quad (2)$$

For the  $k$ th lamina of a piezo-composite laminate, the stress components are

$$\begin{Bmatrix} \sigma_x \\ \sigma_y \\ \tau_{xy} \end{Bmatrix}^k = \begin{Bmatrix} Q_{11} & Q_{12} & Q_{16} \\ Q_{12} & Q_{22} & Q_{26} \\ Q_{16} & Q_{26} & Q_{66} \end{Bmatrix}^k \times \left\{ \begin{Bmatrix} \varepsilon_x^0 \\ \varepsilon_y^0 \\ \gamma_{xy}^0 \end{Bmatrix} + \begin{Bmatrix} \kappa_x^0 \\ \kappa_y^0 \\ \kappa_{xy}^0 \end{Bmatrix} z - \begin{Bmatrix} d_x \\ d_y \\ d_{xy} \end{Bmatrix} E_z - \begin{Bmatrix} \alpha_x \\ \alpha_y \\ \alpha_{xy} \end{Bmatrix} \Delta T \right\} \quad (3)$$

where  $[\bar{Q}_{ij}]$  is the transformed reduced stiffness matrix of the laminate. By

integrating Eq.(3), for all the lamina of the laminate, we obtain

$$\begin{bmatrix} A & B \\ B & D \end{bmatrix} \begin{Bmatrix} \varepsilon^0 \\ k \end{Bmatrix} = \begin{Bmatrix} N + N^a + N^T \\ M + M^a + M^T \end{Bmatrix}^k \quad (4)$$

where  $A$ ,  $B$ , and  $D$  are the extensional, coupling and bending stiffness matrix respectively, and  $N$  and  $M$  are the extensional mechanical resultant force and moment,  $N^a$  and  $M^a$  are the resultant electro-active force and moment,  $N^T$  and  $M^T$  are the thermal forces and moment. From Eq.(4), the equivalent elastic modulus of the piezoelectric actuator can be calculated as  $E = 92.2$  GPa,  $G = 35.7$  GPa; the bending and torsional rigidity as  $EI = 0.0268$  Nm<sup>2</sup>;  $GJ = 0.042$  Nm<sup>2</sup>.

For a basic beam element, the relationship between force and displacements can be described as:

$$\{H\} = [F]\{P\} \quad (6)$$

where  $\{H\}$  is displacement vector in 6 DOF, and  $\{P\}$  is force vector, and  $[F]$  is a 6x6 flexibility matrix of a beam element.

The stiffness matrix is given by

$$[E] = [C]^T [F]^{-1} [C] \quad (7)$$

where  $[C]$  is the coordinate transformation matrix, and  $[ ]^T$  indicates matrix transposition.

After forming the total system stiffness matrix  $[E]$  and mass matrix  $[M]$ , we obtain the vibration governing equation

$$[E]\{v_k\} = \lambda_k [M]\{v_k\} \quad (8)$$

The system vibration frequencies were obtained by solving the above equation.

The resonant frequencies of the structure were then calculated based on a beam element model with the above properties. The piezoelectric actuator was modelled as a curved cantilevered beam, which has 19 nodes and 18 elements. The nylon joint flexure was modelled as an arc with 7 nodes and 6 beam elements. The angle of each arc was half of angle between the two bars L1 and L2. The wing is modelled as a

beam with 10 nodes and 9 elements. Compared to the flexural and piezoelectric actuator, the carbon bars have much higher stiffness. So we assumed that one end of the flexural is fixed. Experiments also showed that the lengths of the linkage bars L1 and L2 had little effect on the resonant frequency of the system. The whole system as shown in Figure 1 is modelled as a 40 nodes and 39 elements beam structure.

The first resonant frequency of the cut actuator calculated as above was 27.5 Hz, which agrees well with the measured value 26.2 Hz. The dome height calculated from the modelling was 7.8 mm, also in good agreement with the measured value of 7.3 mm. This indicates that the simple beam element model can approximate the actuator well. The resonant frequencies of the whole system including the linkage bars, flexural joint, and the attached wing were then calculated in the same way.

### **3.2 Characterization of the 2-bar 2-flexure mechanism**

Table 2 summarises the calculated and measured fundamental resonant frequencies of a system with the flexure joint of 6 mm long and 3 layers of nylon as functions of the angle between the 2 bars L1 and L2. Since the 3 layers of nylon were glued together using superglue (Cyanoacrylate) therefore the exact thickness, stiffness and bending stiffness of this 3-layer flexure was not known. The calculation was carried out by validating and adjusting the bending stiffness of the 3-layer nylon flexure joint at 90° to make the predicted fundamental resonant frequency agree with the measured value (18.04 Hz). Based on the validated analytical model, the fundamental frequency for the rest of flexure joint setting angles was then calculated to compare with the test data in Table 2. Both the predicted and measured results show that the fundamental resonant frequency decreases with the increasing angle between the 2 bars. The results indicate that the measured and the calculated values have a very good

agreement for the flexure joint setting angle larger than 90°. For the joint angles smaller than 90° however, the measured frequencies are higher than the calculated ones. For the case of joint angle at 90°, the effect of changing the flexure length and thickness on the fundamental resonant frequency of the system are summarised in Table 3. From the table it is clear that the resonant frequency increases with increasing thickness and decreasing length of the nylon flexure.

Based on the stiffness and frequency of the system with 3-layer flexure joint, the stiffness and frequencies of the system with 1-layer and 2-layer flexure joints were calculated. Although the variation of the joint layer has little effect on the total mass of the system, it has a significant effect on the fundamental frequency since the rest of the system components were much stiffer. In this case, the system can be simplified as a single DOF model in which the stiffness and frequency of the 3-layer system are represented by  $k$  and  $\omega_{3-L} = (3k/m)^{1/2}$ . Based on this simplified model, the frequency of the 1-layer and 2-layer system were approximated by  $\omega_{1-L} = (k/m)^{1/2}$  and  $\omega_{2-L} = (2k/m)^{1/2}$  respectively with the predicted results listed and compared with the measured data in Table 3. The obtained approximation values (i.e.  $18/\sqrt{3}=10.39$ ) are very close to the calculated value (10.94) using beam element model, as listed in the Table.

Figure 2 (a) shows the measured resonant frequencies for systems of the 3-layer nylon flexure with different length of 4, 6 and 7 mm as function of the joint angle between the two bars L1 and L2. Generally, the trend agrees with the modelling results, i.e., the fundamental resonant frequency increases with the decreasing flexure length and the joint angle between the two bars. However, for a few points of the 4 mm flexure

the measured frequencies were smaller than those of the 5 mm flexure. Most probably this was due to experimental errors which may arise due to the uncertainty to keep consistent clamping conditions when changing the joint angles. The wing tip displacements for the above mechanisms as function of the joint angle are shown in Fig. 2 (b). Generally speaking, the wing tip displacement decreases with the decreasing flexure length and the joint angle.

From the above results it is clear that neither the resonant frequency  $f$  nor the tip displacement  $A$  is enough to characterise the performance of the actuator for the MAV application. A longer flexure can achieve a larger tip displacement and therefore the flapping motion, but the longest flexure is not necessarily the best option for the MAV application. The power output of the actuator and the aerodynamic efficiency of the wing are proportional to the flapping frequency. We introduce the frequency multiplied by tip displacement of the wing ( $f * A$ ) as a performance criterion for the actuated wing structure. Therefore the aim becomes to obtain the maximum  $f * A$  for the actuator optimization. Fig. 2 (c) shows  $f * A$  as a function of the joint angle for the same system. It can be observed that the largest  $f * A$  existed for the 3-layers and 6 mm long flexure when the angles between the two bars lie in 40-60°.

When the flexure thickness was changed to 2-layer or 1-layer nylon, generally the tip displacements were increased and resonant frequency decreased, the measured first resonant frequencies for the mechanisms with the 2-layer and 1-layer nylon flexure when the angle between the two bars was 90° are listed in Table 3. It can be observed from table 3 that measured data agrees qualitatively with the calculated ones, i.e., the resonant frequency decreases with the increasing flexure length and decreasing

thickness, however the measured frequencies were lower than the calculated ones, especially for the 1-layer flexures. We believe this is mainly due to the way the thickness and the bending rigidity constant  $EI$  of the 2-layer and 1-layer flexures were obtained from that of 3-layer flexure. The 3-layer flexure was consisted of 3 layers of nylon and 2 layers of the glue, and its Young's modulus  $E$  was adjusted so that the calculated resonant frequency equals the measured value 18 Hz. The 2-layer flexure was consisted of 2 layers of nylon and 1 layer of the glue but its bending stiffness was assumed equal to  $2/3$  for the 3-layer flexure, which over-estimated its bending stiffness. The 1-layer flexure contained no glue layer but its bending rigidity was assumed equal to  $1/3$  of the 3-layer flexure's bending stiffness, which greatly over-estimated its bending rigidity. Fig. 3 shows the measured  $f^*A$  values for the systems with 1 layer nylon flexure of different lengths and different joint angles between the two bars. The largest  $f^*A$  value (0.378) was marked smaller than the largest  $f^*A$  value (0.777) for the system with 3-layer flexure.

#### **4 Conclusions**

We have introduced  $f_r^*A$  as an optimization criterion for analysing piezoelectric motion amplification mechanisms where  $f_r$  is its fundamental resonant frequency of the system and  $A$  the vibration amplitude at the wing tip, or the free tip deflection at quasi-static operation. This criterion can be used to design a piezoelectric actuation mechanism with the best energy transmission coefficient for flapping wing MAV applications, and is a measurable quantity therefore can be compared with experimental results. Optimal design according to this criterion has been carried out for a number of the 2-bar 2-flexure mechanism configurations, such as the length and the thickness of the flexure, as well as the joint angles between the two bars.

The fundamental resonant frequencies of the piezoelectric actuated system have been calculated by modelling the actuator as a composite laminate and the system as a beam structure. The calculated values were compared with the measurement results. Generally speaking good agreements have been obtained between the calculated and the measured ones, suggesting the composite laminate and beam model is a very simple and helpful means in the future investigation of motion amplification mechanisms for MAV applications. Reasons for discrepancy between them have been discussed.

### **Acknowledgements**

This work was financially supported by the UK EPSRC Grant Flapping Wing MAV EP/C511190/1 and Platform Grant EP/D506638/1.

## References

- <sup>1</sup> W. Shyy, M. Berg and D. Ljungqvist, Prog. in Aerospace Sci. **35** (1999) 455-505.
- <sup>2</sup> C.P. Ellington, Journal of Experimental Biology, **202** (1999) 3439-3448.
- <sup>3</sup> C. Niezrecki, D. Brei, S. Balakrishnan, and A. Moskalik, The shock and vibration digest. **33** (2001) 269-280.
- <sup>4</sup> R.S. Fearing, K.H. Chiang, M.H. Dickinson, D.L. Pick, M. Sitti, and J. Yan, Wing transmission for a micromechanical flying insect, in: Proc. IEEE Int. Conf. Robotics and Automation, San Francisco, CA, USA, 2000, pp. 1509-1516.
- <sup>5</sup> M. Sitti, PZT actuated four bar mechanism with two flexible links for micromechanical flying insect thorax, in: IEEE Int. Conf. Robotics and Automation, South Korea, 2001, pp.3893-3900.
- <sup>6</sup> J. Yan, R.J. Wood, S. Avadhanula, M. Sitti, and R.S. Fearing, Towards flapping wing control for a micromechanical flying insect, in: IEEE Int. Conf. Robotics and Automation, South Korea, 2001, pp.3901-3908.
- <sup>7</sup> A. Cox, D. Monopoli, D. Cveticanin, M. Goldfarb, and E. Garcia, J. Intelli. Mat. Syst. and Struct. **13** (2002) 611-615.
- <sup>8</sup> H.C. Park, K. J. Kim, S. Lee, S. Y. Lee, Y. J. Cha, K. J. Yoon, and N. S. Goo, Biomimetic Flapping Devices Powered by Artificial Muscle Actuators, in: UKC2004 US-Korea Conference on Science, Technology and Entrepreneurship, August, 2004.
- <sup>9</sup> Q. Wang and L.E. Cross, Ferroelectrics, **215** (1998) 187-213.
- <sup>10</sup> Q. Wang, X. Du, B. Xu and L.E. Cross, IEEE trans. on Ultrason. ferro. freq. contr., **46** (1999) 638-646.
- <sup>11</sup> R. M. Alexander, Principles of Animal Locomotion, Princeton Uni. Press, Princeton, 2003.

- <sup>12</sup> G. Taylor, R. Nudds and A. Thomas, *Nature*, **425** (2003) 707-711.
- <sup>13</sup> Hsien-Chun Chung, K. Lal Kummari, S. J.Croucher, N. J.Lawson, S. Guo, R.W. Whatmore, and Z. Huang, *Sensors and Actuators*, **A149**, (2009) 136-142.
- <sup>14</sup> D. J. Inman, *Engineering Vibration*, Prentice hall International, New Jersey, 2001.
- <sup>15</sup> K. J. Yoon, K. H. Park, S. K. Lee, N. S. Goo, and H. C. Park. *Smart Mater. Struct.* **13** (2004) 459-467.
- <sup>16</sup> S. Aimmanee and M. W. Hyer, *Smart Mater. Struct.* **13** (2004) 1389-1406.

## Figure Captions

- Fig. 1 The schematic set up of the piezoelectric actuated motion amplification mechanism for flapping wing MAV application.
- Fig. 2 The measured properties as functions of the joint angle between the two bars L1 and L2 for systems with 3-layer nylon and different flexure length of 4, 6 and 7 mm. (a) Resonant frequency  $f$ ; (b) wing tip displacement  $A$ ; and (c)  $f^*A$ .
- Fig. 3 The measured  $f^*A$  as a function of the joint angle between the two bars L1 and L2 for systems with 1-layer nylon and different flexure length of 2, 3, 4, 5 and 6 mm.

Table 1: Summary of the material parameters used

	Piezoelectric ceramic	Aluminum foil	Stainless steel	Adhesive Layer	Carbon Fibre	Nylon
Young's Modulus E (GPa)	67	70	190	3.45	130	1.02
Shear Modulus G (GPa)	25.57	26.9	75	1.48	5	1
Poisson ratio $\nu$	0.31	0.3	0.3	0.4	0.3	0.4
CTE ( $10^{-6} \text{ }^\circ\text{C}^{-1}$ )	3	23.4	17.3	45		
Density ( $10^3 \text{ Kg m}^{-3}$ )	7.8	2.7	8		1.9	1.1
Thickness (mm)	0.25	0.025	0.19	0.0775	0.65	0.12

Table 2: Summary of the calculated and measured first resonant frequency for the system with the flexure joint of 6 mm long and 3 layers of nylon as functions of the angle between the 2 bars L1 and L2.

Angle (deg)	Calculated	Measured
40	18.8	22.8
50	18.54	22.4
60	18.39	22.2
70	18.24	21.6
80	17.99	19.9
90	18.04	18
100	17.72	17.7
110	17.61	
120	17.54	17.8
130	17.32	
140	17.28	17.2

Table 3: Summary of the calculated and measured first resonant frequency for systems with different flexure length and thickness when the angle between the 2 bars L1 and L2 was 90°.

	4 mm	6 mm	7 mm
3-Layer calculated	21.27	18.04	16.92
3-Layer measured	19.7	18	16.2
2-Layer calculated	17.57	14.97	14.09
2-Layer measured	14.6	14.1	
1-Layer calculated	12.66	10.94	10.39
1-Layer measured	5.5	3.9	

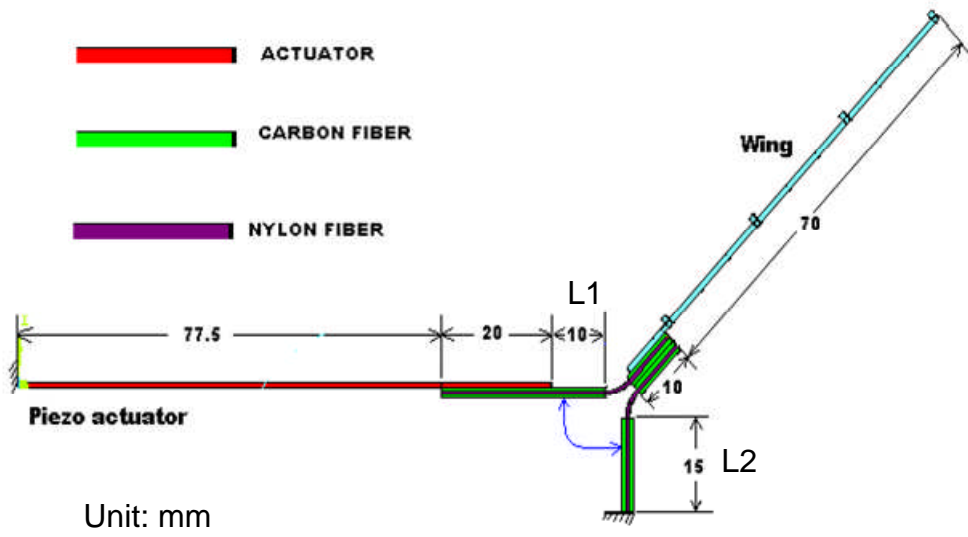


Fig. 1

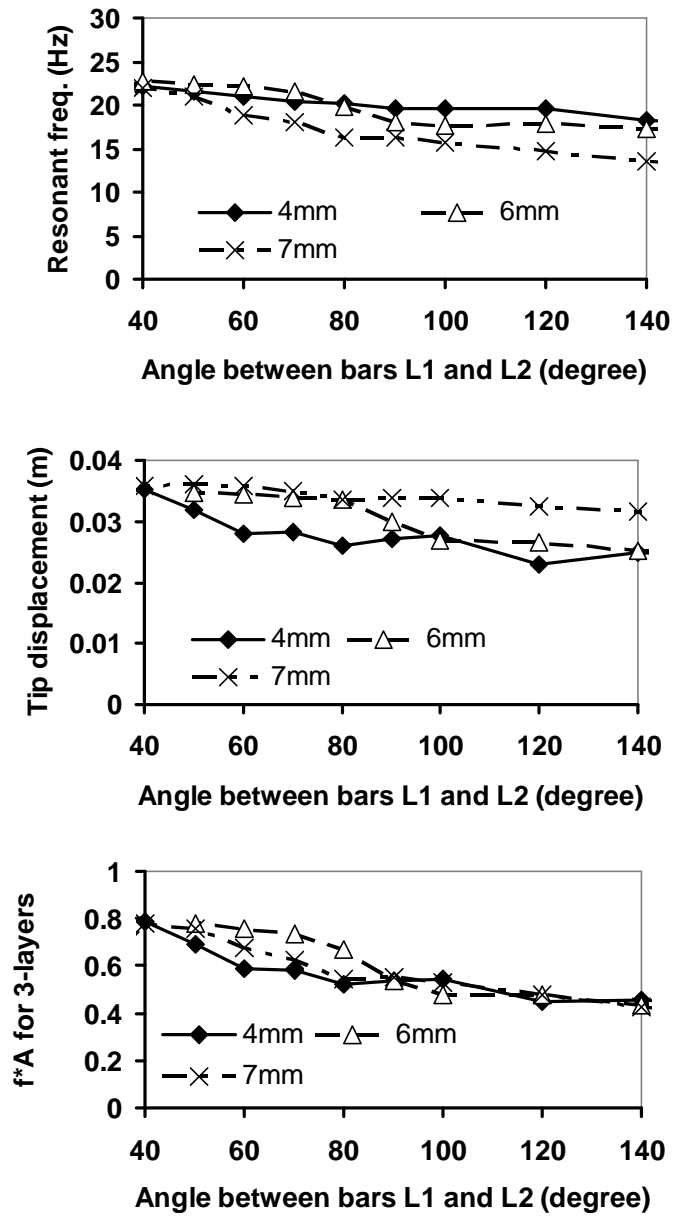


Fig. 2

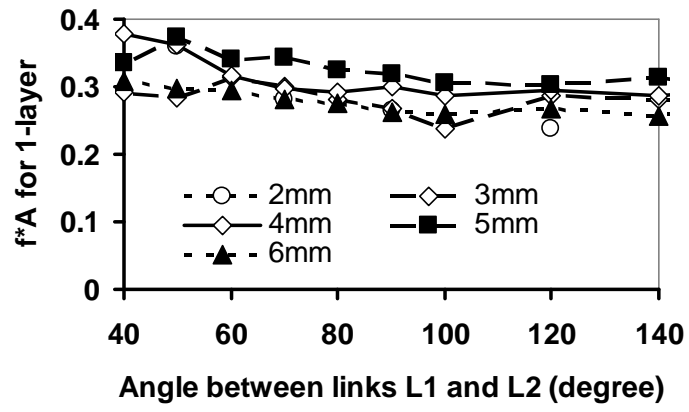


Fig. 3